HHS Public Access

Author manuscript

J Chem Theory Comput. Author manuscript; available in PMC 2019 September 16.

Published in final edited form as:

J Chem Theory Comput. 2019 February 12; 15(2): 1440–1452. doi:10.1021/acs.jctc.8b01107.

Effects of All-Atom Molecular Mechanics Force Fields on Amyloid Peptide Assembly: The Case of Aβ_{16-22} Dimer

Viet Hoang Man[†], **Xibing He**[†], **Philippe Derreumaux**[‡], **Beihong Ji**[†], **Xiang-Qun Xie**[†], **Phuong H. Nguyen**[‡], **Junmei Wang**[*,†]

[†]Department of Pharmaceutical Sciences, School of Pharmacy, University of Pittsburgh, Pittsburgh, Pennsylvania 15261, United States

[‡]Laboratoire de Biochimie Théorique UPR 9080, CNRS, Université Denis Diderot, Sorbonne Paris Cité, IBPC, 13 Rue Pierre et Marie Curie, 75005 Paris, France

Abstract

We investigated the effects of 17 widely used atomistic molecular mechanics force fields (MMFFs) on the structures and kinetics of amyloid peptide assembly. To this end, we performed large-scale all-atom molecular dynamics simulations in explicit water on the dimer of the seven-residue fragment of the Alzheimer's amyloid-β peptide, Aβ16−22, for a total time of 0.34 ms. We compared the effects of these MMFFs by analyzing various global reaction coordinates, secondary structure contents, the fibril population, the in-register and out-of-register architectures, and the fibril formation time at 310 K. While the AMBER94, AMBER99, and AMBER12SB force fields do not predict any β-sheets, the seven force fields, AMBER96, GROMOS45a3, GROMOS53a5, GROMOS53a6, GROMOS43a1, GROMOS43a2, and GROMOS54a7, form β-sheets rapidly. In contrast, the following five force fields, AMBER99-ILDN, AMBER14SB, CHARMM22*, CHARMM36, and CHARMM36m, are the best candidates for studying amyloid peptide assembly, as they provide good balances in terms of structures and kinetics. We also investigated the assembly mechanisms of dimeric Aβ16−22 and found that the fibril formation rate is predominantly controlled by the total β-strand content.

Graphical Abstract

[*]**Corresponding Author:** junmei.wang@pitt.edu.

Supporting Information

The Supporting Information is available free of charge on the ACS Publications website at DOI: 10.1021/acs.jctc.8b01107. Statistical data of the conformational states (Tables S1 and S2), the 100 initial structures of Aβ_{16-22} (Figure S1) and the distribution of some their parameters (Figure S2), intermolecular interaction maps (Figures S3−S5), evidence for convergence of conformational sampling (Figure S6), and time evolution of the reaction coordinates including secondary structural contents, intermolecular interactions, P2, cosine, and gyrate radii of the dimer (Figures S7 and S8) (PDF)

The authors declare no competing financial interest.

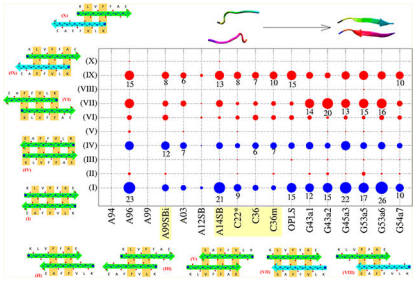

INTRODUCTION

Biomolecules are complex systems. Their structures are represented by multidimensional rugged energy landscapes with a huge number of local minima separated by high energy barriers. Therefore, adequate description of the atomistic interaction or force field and convergence of the configuration space sampling of such a complex energy landscape are two primary concerns of any simulation studies. The efficient sampling can be obtained with enhanced conformational search techniques such as replica exchange molecular dynamics (REMD),[1] simulated tempering,[2] and metadynamics[3] or with multiple molecular dynamics (MD) trajectories starting from different initial configurations. The quality of a force field is validated by the experimental values of the properties the force field predicts. Currently, there are four widely used force field families for MD simulations of proteins and peptides, including AMBER,[4] CHARMM,[5] GROMOS,[6] and OPLS.[7] The existing classical force fields have been under continuous improvement and verification; however, their successful applications to many systems remain to be validated due to the complexity of the energy landscape. Thus, one may always ask how the employed force field affects the simulation results.

The influence of the force fields on the equilibrium structures of non-amyloid peptides has already been reported.[8–13] Extensive force field refinements aimed at obtaining better agreements of the simulated structures, dynamics, and thermodynamics of single proteins with experiments have also been carried out.[14] However, for the amyloid peptides which undergo aggregation forming oligomers and fibrils, the validation of the force fields is much more difficult owing to the lack of experimental data on the transient oligomers. Among many amyloid peptides, the Aβ peptides and truncated variants have been extensively discussed in their monomeric forms using various force fields because of their importance related to Alzheimer's disease.[15–24] In the context of oligomers, a majority of simulations have been carried out using individual force fields, but few studies aimed at comparing force fields for the Aβ dimer and trimer.[24–27] Table 1 summarizes recent publications on comparing the different force fields for studying Aβ peptides in explicit water.

The enhanced sampling method REMD has been extensively used in these studies to ensure sampling convergence. Simulation results can be validated by comparing to experimental data such as secondary structure, chemical shifts, CD spectrum, residual dipolar couplings, NMR spectrum, and collision cross sections. These computational studies provided valuable insights into the effects of various force fields on the secondary and tertiary structures, the stability, and population of the fibril-prone conformations. However, for a given system,

only a few force fields are tested and the simulation time scales, data analysis methods, and targeted experimental measurements are also different; thus, it is difficult to compare the computational results with high confidence. Moreover, these studies mainly focus on the structure of the Aβ peptides, and to the best of our knowledge, there is only one publication studying the effect of atomistic force fields on the kinetics of the amyloid aggregation.[27] With this in mind, in this work, we carry out large-scale comparison of 17 widely used atomistic force fields on the structures and kinetics of the dimer formed by the seven-residue fragment Aβ_{16-22} of the full length Aβ peptide. The considered force fields include (i) seven members of the AMBER family, AMBER94 (A94),[4] AMBER96 (A06),[28] AMBER99 (A99),[29] AMBER99SB-ILDN (A99SBi),[30] AMBER03 (A03),[31] AMBER12SB (A12SB),[32] and AMBER14SB (A14SB),[32] (ii) three members of the CHARMM family, CHARMM22* (C22*),[33] CHARMM36 (C36),[34] and CHARMM36m (C36m),[35] and (iii) six members of the GROMOS family, GROMOS-43A1 (G43a1),[36] GROMOS-43A2 (G43a2),[37] GROMOS-45A3 (G45a3),[38] GROMOS-53A5 (G53a5),[39] GROMOS-53A6 (G5a6),[39] GROMOS-54A7 (G54a7),[40] and (iv) OPLS-AA (OPLS).[7] The total MD simulation for the 17 force fields is 0.34 ms. This time scale requires much more time and computer resources if the full length Aβ_{1-40} or Aβ_{1-42} peptides are simulated; particularly the oligomerization of the full-length Aβ peptides needs a much longer simulation time to reach the convergence in comparison with the oligomerization of shorter peptides. The Aβ_{16-22} segment containing the central hydrophobic core (residues 17−21) is not sufficient to fully understand the whole Aβ peptides, as aggregation kinetics vary between Aβ40 and Aβ42, but it is essential for fibrillization of full-length amyloid-beta proteins. Thus, it is an appealing model system for physical studies of fibril formation.[41–44] It helps to explore fundamental aspects of the thermodynamics and kinetics of amyloid aggregation.[45,46] Moreover, the ability of this peptide to form fibrils in vitro with antiparallel ordering of the β-strands was ascertained by solid-state NMR.[47] Thus far, small aggregates of this peptide have only been studied computationally by either an all-atom representation with limited sampling of configuration space[48–51] or extensive simulations with simplified protein models.[52–57] Overall, we still lack of a full understanding of the dependence of the structures and aggregation kinetics of this peptide on the force field. On the basis of our results and the previously published works, we conclude that only 5 (A99SBi, A14SB, C22*, C36, and C36m) out of 17 force fields studied in this work are the top candidates for the simulation of amyloid aggregation. These force fields yield a good balance between the populations of fibril and disordered states and capture the picture of the solid-state NMR antiparallel in-register and out-of-register β-sheet distributions as a function of pH for Aβ fragment fibrils. Additionally, by using 100 MD trajectories, we can estimate the fibril formation time of the Aβ peptides for each force field. We also show that among all possible collective variables the fibril formation rate is predominantly correlated to the β-strand content of chains.

MATERIALS AND METHODS

Force Fields.

The effective potential energy function shown below is employed by most classical force fields for biomolecular simulations

$$V = \sum_{\text{bonds}} K_r\left(r - r_{\text{eq}}\right)^2 + \sum_{\text{bonds}} K_\theta\left(\theta - \theta_{\text{eq}}\right)^2 + \sum_{\text{dihedrals}} \frac{V_n}{2}\left[1 + \cos\left(n\phi - \delta_n\right)\right] + \sum_{i<j}\left[\frac{A_{ij}}{R_{ij}^{12}} - \frac{B_{ij}}{R_{ij}^{6}} + \frac{q_i q_j}{\varepsilon R_{ij}}\right] \quad (1)$$

Here, the first two terms describe the harmonic potentials associated with the bond stretching and bond angle bending, respectively, and the torsional angle twisting is described by a Fourier expansion in the third term. As for the nonbonded energy terms, the van der Waals and electrostatic interactions are treated by the Lennard-Jones 12−6 potential and Coulomb potential, respectively. Force fields are different in both the parameters that describe the energetic components and the parametrization strategies to derive these parameters. A general discussion on the various force-field parametrization procedures and developments is detailed elsewhere.[4–7] Briefly, the AMBER family starts with A94[4] followed by A96,[28] where the (ϕ/ψ) torsional potentials were adjusted to yield better agreement between molecular mechanical and quantum mechanical energetics. The next version, A99, was introduced on the basis of A94 with new torsional parameters.[29] Modifications in the potential of the peptide backbone torsional angles and specifically of the side-chain torsional angles of four amino acids Ile, Leu, Asp, and Asn result in A99SBi.[30] A03 is different from the A94/A99 series, where the main-chain torsional potentials and charges were rederived.[31] The A12SB[32] and A14SB[32] are two revised versions of the A99SB force field with modified torsions of backbone and side chains, producing better measurements compared with experiments. The CHARMM family includes CHARMM22[5] originally developed for nucleic acids and later on was extended to handle peptides. Its descendant C22* was introduced with modifications in partial charges of the Asp, Glu, and Arg and backbone torsional angles.[33] The next version C36 was introduced with major improvements over C22*, including refined backbone CMAP potentials which describe the (ϕ/ψ) dihedral angle cross-term, and new side-chain dihedral parameters.[33] The most recent version C36m, based on a refined backbone CMAP potential and derived from reweighting calculation and a better description of specific salt bridge interactions, improves the accuracy of the conformational ensemble of intrinsically disordered peptides and proteins.[35] For the OPLS force field, the bond stretching and angle bending terms were mostly taken from A94 except for alkanes, for which the parameters were taken from CHARMM22. All torsional and nonbonded parameters were reoptimized to reproduce conformational energetics, gas-phase intermolecular energetics, and thermodynamic properties of pure liquids. Finally, the GROMOS family differs from the other families by employing a united atom approach representing each of the nonpolar CH, CH_2, and CH_3 groups as a single particle. The G43a1 was introduced in 1996,[58] and G43a2 was evolved from G43a1 by modifying some torsional-angle parameters and adding third-neighbor van der Waals interactions to better reproduce the distribution of the torsional-angle values in short aliphatic chains.[37] However, the densities of long alkanes predicted by this force field are too high, so G43a2 was then upgraded to G45a3 with two additional atom types for branched and cyclic alkanes and a reparameterization of the aliphatic united atoms.[38] Next,

the G53a5 and G53a6 force fields are the result of a complete reparameterization of the nonbonded interaction parameters for condensed phase simulations of pure liquids of small molecules (G53a5) and solutions of molecular systems in water or nonpolar solvents (G53a6).[39] The G54a7 was introduced on the basis of G53a6 with new ϕ/ψ torsional angle terms and a modification of the N-H, C=O repulsive term to correct the 53A6 helical propensities.[40]

Simulation Details.

Following our previous study,[24] the simulated sequence, Lys-Leu-Val-Phe-Phe-Ala-Glu (KLVFFAE), is free of capped ends at pH 7. Starting from the configuration of a monomer, extracted from the NMR structure of the $A\beta_{10-35}$ peptide (PDB code: 1HZ3),[59] we carried out a 100 ns MD simulation employing the A99SBi force field and the TIP3P water.[60] The 5000 structures of the last 50 ns were selected and placed randomly in space, resulting in 100 dimeric structures, as shown in Figure S1 of the Supporting Information.

These dimer structures were placed in periodic octahedral boxes containing about 1955 water molecules, with a peptide concentration of 53.6 mM. The explicit water models mTIP3P, TIP4P, and SPC were used for C22*, OPLS, and the GROMOS force field family, respectively. The TIP3P water model was used for the other force fields. The solvated systems were then minimized using the steepest descent method and were equilibrated for 1 ns at a constant pressure of 1 atm using the Berendsen coupling method[61] and at a temperature of T = 310 K controlled by the Bussi−Donadio−Parrinello velocity scaling method.[62] The systems were subsequently equilibrated at constant temperature (T = 310 K) and constant volume (NVT) for 1 ns. The final structures were used as the starting configuration for 200 ns NVT MD simulations at 310 K. For each force field, we carried out 100 MD trajectories starting from different disordered structures of the dimer, and each trajectory lasted for 200 ns, resulting in 20 μs (μs) in total.

All of the MD simulations were performed with the GROMACS 4.5.5 package.[63] Integration of the equations of motion was conducted using the leapfrog algorithm[64] with a time step of 2 fs. The LINCS algorithm[65] was used to constrain the lengths of all covalent bonds with a relative geometrical tolerance of 10^{-4}. The van der Waals forces were calculated with a cutoff of 1.0 nm, and the particle mesh Ewald method[66] was employed to treat the electrostatic interactions. The nonbonded interaction pair list, with a cutoff of 1.0 nm, was updated every 5 fs.

Data Analysis.

Structural Characterization.—Self-assembly is characterized by the total number of intermolecular side chain−side chain contacts (N^{sc}_C) and intermolecular backbone hydrogen bonds (N^{hbond}_C). A side chain−side chain contact is formed if the distance between the centers of mass of two residue side chains is within 6.5 Å. A hydrogen-bond (H-bond) is formed if the acceptor−donor distance is within 3.5 Å and the acceptor−donor−H angle is less than 30°. The secondary structure contents (β, helix, and coil) were calculated using the STRIDE algorithm.[67,68] Here, the helix content includes 3−10 helix, Pi helix, and α-helix, the β-content consists of extended residues, and the rest is coil one. The nematic order

parameter (P_2)[50,69] was used to characterize the fibril states. The end-toend distance (d_{ee}) between the Cα atoms of the first and last residues of each chain was examined. The radii of gyration (R_g) and solvent accessible surface areas (SASAs) were calculated using the GROMACS tools.

Disordered, Intermediate, and Fibril States.—To characterize Aβ_{16-22} aggregation, we classified the dimer conformations into three states: disordered, intermediate, and fibril-like states. We used both the order parameter (P_2) and β-sheet content to characterize the three main states. A β-sheet structure of the dimer is recognized when two β-strands (one for each monomer) are connected laterally by at least two backbone H-bonds, to form a generally twisted, pleated sheet. The β-strand is a stretch of polypeptide chain two to five residues long with the backbone in an extended conformation. A structure will be in the fibril state if it forms a β-sheet structure with $P_2 \geq 0.8$ or in the disordered state if it does not contain a β-sheet structure or its $P_2 \leq 0.5$; or in the intermediate state if it does not belong to the first two categories. The fibril state is further characterized by parallel and antiparallel orientations of β-sheets. To determine whether it is parallel or antiparallel, a vector which has its origin at the C_α of the starting residue and the arrowhead at the C_α atom of the ending residue is created for each β-strand. The β-sheet is parallel if the cosine of the angle between the two β-strand vectors is positive and antiparallel otherwise.

Fibril Formation Time and Fibril Dissociation Time.—We introduced the fibril formation time and fibril dissociation time, τ, which is calculated with eq 2. The fibril formation time is the time for a disordered dimer to reach the fibril state, while the fibril dissociation time is the time a dimer stays in a β-sheet structure until it dissociates into monomers.

$$\tau = \frac{\sum_{k=1}^{N} \tau_k}{N} \quad (2)$$

In calculation of the fibril formation time, τ_k is the first passage time that the kth trajectory reaches the fibril state and N is the total number of trajectories that reaches the fibril state within 200 ns. In the calculation of fibril dissociation time, τ_k is the average of all of the fibril dissociation times in the kth trajectory.

RESULTS

The Overall Structure.

To obtain a first impression on the overall structures of Aβ_{16-22} dimer sampled by the 17 force fields, we show in Figure 1 the distribution of various global reaction coordinates including R_g, d_{ee} of monomers, P_2, the total number of intermolecular backbone H-bonds N^{hbond}_C, the total number of intermolecular side chain−side chain contacts N^{sc}_C, and SASA. For the AMBER force field family, A94 and A99 give similar overall structures as their global reaction coordinates are comparable: compact ($R_g \approx 0.68$ nm), nonextended monomer ($d_{ee} \approx 1$ nm), disordered ($P_2 \approx 0.3$), and a small number of interchain contacts

($N^{hbond}_C \approx 1$, $N^{sc}_C \approx 4$). The other members A96, A99SBi, and A14SB show dominant single peaks in their distributions corresponding to ordered dimers with extended chains and many interchain contacts ($R_g \approx 0.80$ nm, $d_{ee} \approx 2$ nm, $P_2 \approx 0.85$, $N^{hbond}_C \approx 3$, and $N^{sc}_C \approx 8$). The other two AMBER force fields, A12SB and A03, are in between these two groups with flat distributions, but A12SB is more similar to A94 and A99, and A03 is closer to A96, A99SBi, and A14SB counterparts. It is notable that the structures of A03 are the most solvated (SASA ≈ 11 nm^2), while the structures of the other AMBER members are less solvated (SASA ≈ 8−9 nm^2).

For the CHARMM force field family, each distribution shows a dominant peak corresponding to the ordered dimer with extended chains ($R_g \approx 0.75$ nm, $d_{ee} \approx 1.9$ nm, $P_2 \approx 0.80$, $N^{hbond}_C \approx 3$, and $N^{sc}_C \approx 9$) and a broad ensemble of much less populated conformational states, corresponding to disordered dimers and nonextended chains ($R_g \approx 0.65$ nm, $d_{ee} \approx 1.0$ nm, $P_2 \approx 0.40$, $N^{hbond}_C \approx 1$, and $N^{sc}_C \approx 3$). All structures sampled by the CHARMM force fields are partially solvated with a SASA around 6.3 nm^2. The overall structures obtained by OPLS are very similar to those by CHARMM members, except their SASAs (≈10 nm^2) are larger.

For the GROMOS force field family, the height of the single peaks of the distributions are much greater than those of the AMBER, CHARMM, and OPLS force fields, indicating that GROMOS force fields sample much more ordered dimers with extended monomers ($P_2 \approx 0.82$, $d_{ee} \approx 1.9$ nm). Indeed, very few dimers free of any interchain contact were sampled by the GROMOS force fields. The overall structures with all GROMOS force fields are highly solvated with SASA ≈ 11 nm^2.

To further characterize the intermolecular interactions, we constructed interaction maps to show the probabilities of the side chain−side chain contacts and backbone H-bond formations between two residues belonging to two chains (see Figures S3−S5 in the Supporting Information). In all of the maps, the high frequent contacts occur at the inverted diagonal region, which indicates antiparallel order of the sampled dimers. As shown in Figures S3−S5, intermolecular interactions are weak for dimer structures sampled by A94, A99, and A12SB and very strong for the structures produced by the GROMOS force field family. The maps also tell us that (1) the A−L contact is significant for all force fields; (2) the K−K and E−E contacts are negligible for all force fields except for A99; (3) the F−F contacts are significant for G43a1, G43a2, G45a3, and OPLS-AA but not for A94, A99, A99SBi, A12SB, C22*, C36, C36m, and G53a5; (4) the most stable E− K contacts are obtained by OPLS. As shown in the H-bond maps (Figures S4 and S5), all of the force fields except for A94, A99, and A12SB have significant numbers of H-bonds between A−L and F^{19}–F^{20}; the H-bond maps of G43a1, G43a2, and G53a5 are similar, and there is a high probability of H-bond formation between E−L. The H-bond maps of C36m and C36 are very similar, as shown in Figure S4.

To compare two force fields, the Pearson correlation coefficients (Pcc) were calculated from the distributions of the reaction coordinates for the force field pair. Figure 2 shows the correlations between all pairs of force fields studied in this work. The following force field pairs show high correlations (averaged Pcc ≥ 0.9), as shown in Figure 2d: A94-A99, A96-

A99SBi, A96-A14SB, A99SBi-A14SB, A03-OPLS, C22*-C36, C22*-C36m, C36-C36m, OPLS-G43a1, OPLS-G43a2, OPLSG45a3, OPLS-G53a5, OPLS-G53a6, and any pair belonging to the GROMOS family. Interestingly, A12SB does not display a high correlation with any of the other force fields.

Secondary Structure.

Figure 3a shows the mean percentage values of the secondary structures found in conformations generated by a force field. Among the 17 force fields, the helix structure is found by four force fields: A94 (30%), A99 (10%), A12SB (3%), and A03 (1%). The β structure is highly sampled by A96 and all GROMOS family members (>50%) but not sampled by A94 and A99 (0%). For the other force fields, the percentages of β structure vary between 10 and 40%. The highest percentage values of coil population, ~89%, were found for A99 and A12SB, while the values are in the range 45−70% for the other force fields. Overall, we can cluster the 17 force fields into four main groups, with the first group strongly favoring the helix structure (A94), the second group (A12SB, A99) biased toward the coil structure, the third group (A03, A99SBi, A14SB, OPLS, and CHARMM family) providing a good balance between β and coil structures, and the fourth group (A96, GROMOS family) tending to overstabilize β structures.

Conformational States and Fibril Formation Times.

Disordered, Intermediate, and Fibril States.—Figure 3b shows the populations of the disordered, intermediate, and fibril states for all of the 17 force fields. The detailed characterizations of the disordered, intermediate, and fibril states are shown in Table S1 of the Supporting Information. Obviously, the populations of these states are highly dependent on the force fields. It is not surprising that A94, A99, and A12SB favor strongly the disordered state (≥80%) because these force fields do not sample β structure (Figure 3a) and exhibit low P_2 and N^{hbond}_C values (Figure 1). Surprisingly, although G54a7 shows high β content and large P_2 and N^{hbond}_C, its intermediate state population is the highest (50%) among all of the force fields and its fibril state population (33%) is much lower than the other GROMOS force fields. In contrast, A96 provides the highest population of the fibril state (71%), although its β content is similar to that of G54a7, and the probability distributions of P_2 and N^{hbond}_C values are shifted to lower values. A03 and the CHARMM family share a similar state population pattern with a high population of the disordered state (43−51%) and a balance between the fibril and intermediate states (21−30%). A99SBi, A14SB, and OPLS show high populations of the fibril (42−53%) and then disordered (32−39%) and intermediate (13−20%) states. The GROMOS family members (except for A54a7) show an opposite trend with 46−65% of the fibril, 27−43% of the intermediate, and 3−16% of the disordered states.

Parallel and Antiparallel β-Sheet Registries.—We analyzed the structure of the fibril state in more detail, focusing on the parallel/antiparallel and in-register/out-of-register architectures. For a dimeric structure, we calculated the cosine of the angle between two vectors linking N- and C-termini of each peptide. Figure 3c shows the average of the cosine value obtained from different force fields. Although A94 and A99 do not sample the fibril state, their negative cosine values indicate that disordered structures also tend to form

antiparallel conformations. The other force fields favor strongly the antiparallel β-sheet conformation, especially A96 and the GROMOS force field family (cosine ≤ −0.8). A detailed analysis of all individual trajectories shows that A94, A12SB, and OPLS do not sample any transient parallel β-sheet conformations in all 100 MD trajectories. For the other force fields, the probability to observe a transition between the parallel β-sheet and the antiparallel β-sheet among 100 trajectories is 38% (G43a2), 28% (G53a5), 25% (G45a3), 19% (G43a1), 11% (A96 and G53a6), 6% (A03 and C36m), 5% (A99SBi, C36, and G54a7), 4% (C22*), 2% (A14SB), and 1% (A99).

Because the antiparallel β-sheet is dominant in the ordered structures for Aβ_{16-22}, we further analyzed the interchain H-bond patterns (HPT) of those β-sheet structures. Theoretically, for a dimer, there are in total of 10 possible antiparallel β-sheet patterns (HPT_I, HPT_{II}, …, and HPT_X) which can be described by $R1 + k \leftrightarrow R2 - k$ β-sheet registries, i.e., interchain H-bonds between residues $R1 + k$ of one chain and $R2 - k$ of another chain. As shown in Figure 4, HPT_I and HPT_{IV} are in-register with the patterns $16 + k \leftrightarrow 22 - k$. The others are out of-register with the patterns: $18 + k \leftrightarrow 22 - k$ for HPT_{II} and HPT_V, $16 + k \leftrightarrow 20 - k$ for HPT_{III} and HPT_{VI}, $17 + k \leftrightarrow 22 - k$ for HPT_{VII}, $19 + k \leftrightarrow 22 - k$ for HPT_{VIII}, $16 + k \leftrightarrow 21 - k$ for HPT_{IX}, and $16 + k \leftrightarrow 19 - k$ for HPT_X. For examples, $k = 0$, 2, 4, and 6 for HPT_I and $k = 1$, 3, and 5 for HPT_{IV}. The relative sizes of the populations of the 10 antiparallel β-sheet registers are shown in Figure 5 for each force field. The out-of-register beta-sheets shifted by more than two residues are expected to be less stable than the in-register sheet because they have fewer interchain backbone hydrogen bonding and side chain side chain interactions. The population of the β-sheet registries is zero for A94 and A99. The β-sheet registries are also rarely observed in A12SB, and its maximum population of the registries is about 1%. The HPT_{II}, HPT_{III}, HPT_V, HPT_{VIII}, and HPT_X registers are not sampled by almost all force fields, while the HPT_I, HPT_{IV}, HPT_{VII}, and HPT_{IX} registers are frequently sampled by all force fields, except for A94, A99, and A12SB. Most force fields sample the in-register HPT_I with population sizes of 21−26% for A14SB, G53a6, A96, and G53a6; 12−17% for G43a1, G43a2, OPLS, and G53a5; and 5−10% for A03, A99SBi, the CHARMM force field family, and G54a7. HPT_I is found in the solid-state NMR structures of the Aβ16−22 assembly at pH 7.4.[44] The in-register HPT_{II} is less frequently formed, and the population sizes are about 12% for A96, A99SBi, and G45a3 and ≤7% for the other force fields. Looking at the out-of-register patterns, HPT_{VII} is explored 20% of the time by G43a2 and about 15% of the time by A96, G43a1, G43a5, G53a5, and G53a6. For HPT_{IX}, similar population sizes of ~15% are obtained using A96, A14SB, OPLS, and G53a5 and smaller populations are sampled by the other force fields (5−10%). Interestingly, it is observed in experiment that external conditions, such as concentration, temperature, pH, and the exact amino acid composition, can easily shift one β-sheet registry to another. Petkova et al. showed that Aβ11−25 fibrils adopt antiparallel beta-sheets with $17 + k \leftrightarrow 20 - k$ registry at pH 7.4 in contrast to $17 + k \leftrightarrow 22 - k$ registry, i.e., HPT_{VII} at pH 2.4.[70] Also, only two patterns (HPT_{VII} and HPT_{IX}) are shifted by one residue compared to the native pattern.

Fibril Formation Time and Fibril Dissociation Time.—Having compared the force fields in terms of structures, we now compare their fibril formation times τ calculated using

eq 2, and the results are shown in Figure 3d. Small values of τ indicate fast fibril formation. For clarity, because A94, A99, and A12SB trajectories do not reach the fibril states within 200 ns, their fibril formation times are not shown in Figure 3d. As seen, all GROMOS force fields achieve the fastest fibril formation with τ varying between 2 ns for G45a3 and 12 ns for G53a3. The four AMBER force fields A96, A99SBi, A03, and A14SB and OPLS reach the fibril state later with τ around 25 ns. The slowest times for fibril formation were observed with CHARMM force fields with τ = 35 ns for C22*, 45 ns for C36m, and 50 ns for C36. We also calculated the fibril dissociation time following the fibril formation, and results are shown in Figure 3d. As seen, the fibril undergoes the association/dissociation within 200 ns, with the dissociation time depending on the force fields. Overall, the shorter the fibril formation time is, the longer the dissociation time is. All GROMOS force fields, A96, and OPLS exhibit slow fibril dissociation with the time being longer than 80 ns for G43a1, G43a2, G54a7, and OPLS and ~140 ns for G53a6. The two AMBER force fields A99SBi and A14SB dissociate faster with time around 66 ns. The three CHARMM force fields and A03 show a balance between the fibril formation and dissociation with the fastest dissociation of 26 ns for A03 and 34−56 ns for the CHARMM force fields.

DISCUSSION

As our aim is to study the effects of force fields on the structural ensemble and kinetics of the Aβ_{16-22} dimer, it is important that the results are not affected by the initial conformations and limited sampling. The diversity of the 100 different dimer structures is validated by the diverse values of the parameters including P_2, in the range from 0.15 to 0.6, the cosine values in the range from −0.6 to 0.4, and the end-to-end distances in the range from 0.45 to 1.05 nm (see Figure S2 in the Supporting Information). Convergence of sampling is assessed by comparing the distribution of six reaction coordinates using three ensemble averages with all 100 trajectories and with 75 and 50 trajectories selected randomly from 100 trajectories. Excellent agreements were observed between results obtained using three ensembles for all reaction coordinates and all of the 17 force fields. Figure S6 shows the results for four representative force fields, namely, A14SB, C36m, OPLS, and G54a7. The convergence of MD simulations was assessed by investigating the time evolution of the reaction coordinates. As seen in Figures S7 and S8, all collective variables reach plateau values after 100 ns. These results give us high confidence of the quality of the sampling and length of the trajectories, allowing us to discuss the similarity and difference between the force fields and to compare our results with those obtained by other works.

As shown above, the effects of force fields on the structures and kinetics of Aβ_{16-22} dimer are quite complicated, depending on the quantities under investigation. Nevertheless, on the basis of our current results together with previous works, we attempt to suggest the most suitable force fields for the simulation of amyloid protein aggregation. We have clustered the 17 force fields into groups on the basis of the similarity of individual quantities including three secondary structures (β, helix, and coil), the three conformational states (disordered, intermediate, and fibril), the relative orientation of the two chains, and the fibril formation time. To obtain a collective picture of the similarity/dissimilarity of force fields, we clustered all force field results with the eight reaction coordinates, employing the k-mean clustering

method. Note that, due to the difference in the magnitude of data, each reaction coordinate is normalized to its maximum value prior to the clustering (Figure S6). We obtain six groups: group 1: A94, A99, A12SB; group 2: A96, G45a3, G53a5, G53a6; group 3: A99SBi, A14SB, OPLS; group 4: G43a1, G43a2; group 5: G54a7; and group 6: A03, C22*, C36, C36m. Our results indicate that the force fields in the first group should not be used for exploring amyloid formation because of their strong biases toward α-helical structures. Groups 2, 4, and 5 could be employed for studying amyloid formation, but results could be strongly biased toward β-sheet and lead to incorrect kinetics. This allows us to narrow the 17 popular force fields down to a list of seven force fields, namely, A99SBi, A03, A14SB, C22*, C36, C36m, and OPLS, which provide good balances in structures as well as in kinetics and, therefore, should be suitable for simulations of amyloid formation. To further justify this recommendation, let us revisit previous simulations of Aβ_{16-22} oligomers and the monomer and dimers of other Aβ peptides.

In the context of the Aβ_{16-22} dimer, Rohrig et al. have shown that A99 leads to an unstable antiparallel β-sheet structure.[71] In our previous extensive REMD simulation, we have shown that A99 strongly favors coil and 3_{10}-helix and G43a1 only reproduces the antiparallel strands.[24] Using the modified AMBER94 force field, Gnanakaran and colleagues obtained six distinct conformations including shifted parallel strand and parallel loop, parallel strand, antiparallel strand, shifted antiparallel strand, cross, and tight cross/lock.[49] Employing the OPEP coarse-grained force field, we have identified in-register and out-of-register parallel and antiparallel strands.[54,72] These structures obtained by OPEP and modified AMBER94 are essentially captured by all force fields in groups 3 and 6. In the context of the Aβ_{16-22} trimer, our previous REMD simulations have shown that A99 also does not form any fibril-like structures and favors strongly coil and 3_{10}-helix. The G43a1 leads to in-register antiparallel strand, out-of-register antiparallel strand, and mixed parallel and antiparallel.[24] These structures are also captured by extensive simulations using 1.3 μs MD with G43a1[50] and by the OPEP force field.[54] However, the population of the extended β-sheet structures is very high with G43a1. Favrin and colleagues employed a homemade implicit solvent all-atom model and found the mixed parallel/antiparallel β-sheets, in-register and out-of-register antiparallel β-sheets.[52] These structures are essentially captured by the OPLS force field,[24] suggesting that the OPEP, modified AMBER94, and force field of Favrin et al. are counterparts with the force fields in groups 3 and 6.

In the context of the Aβ40/42 monomers, many force field comparison studies have been carried out. Using MD simulations with A03, CHARMM22+CMAP,[73,74] G53a6, G54a7, and OPLS on the Aβ40 peptide, Gerben et al. have shown that G53a6, G54a7, and OPLS lead to similar results, which are consistent with experimental data, while the results from A03 and CHARMM22+CMAP are in conflict with experiments.[18] Somavarapu et al. have studied the structure of Aβ40 monomer using 10 force fields—A03, A99SBi, CHARMM27,[75] C22*, OPLS, OPLS-2006,[76] OPLS-2008,[77] G43a1, G53a6, and G54a7—together with three water models—SPC,[78] TIP3P, and TIP4P.[60] They show that A99SBi and C22* provide the ensembles in the best agreement with available NMR and CD data.[19] Garcia et al. performed extensive REMD simulations of the Aβ40 and Aβ42 monomers and found that A99SBi, C22*, and OPLS led to ensembles in agreement with experiment.[20] Carballo-Pacheco and Strodel calculated the local NMR observables of the Aβ42 monomer

using the five OPLS, AMBER99SB,[79] AMBER99SB*,[30,33,80] A99SBi, AMBER99SBILDN-NMR,[81] and C22* force fields, and all force field results were in good agreement with experiment, except for those using AMBER99SBILDNNMR.[21] Shaw et al. performed benchmark on Aβ40 monomer by considering backbone chemical shifts, NMR data, and the gyrate radii for six force fields including A99SBi, C22*, C36m, AMBER99SB*ILDN, AMBER99SB-UCB, AMBER03WS,[82] and AMBER99SB-disp.[23] They suggested a rank of the applicability of these force fields for Aβ simulations: C36m > AMBER99SB-disp = C22* > AMBER99SB-UCB > A99SBi > AMBER03WS > AMBER99SB*ILDN.[23] Overall, all of these simulation results (except those obtained by Gerber using the GROMOS force field) are consistent with our present findings on Aβ_{16-22} dimer.

In the context of the Aβ oligomers, previously we characterized the high-resolution structures of the Aβ42 dimer by 400 ns REMD simulations and found that the four A99SBi, A14SB, C22*, and OPLS force fields led to random coil ensembles but only OPLS and A99SBi provide good agreement with CD-derived secondary structure contents.[26] Watts and colleagues have compared the performance of five force fields A99SBi, AMBER99SB*, AMBER99SBILDNNMR, C22*, and C36 on the Aβ40 dimer by 300 ns REMD simulations.[34] They have shown that A99SBi and C36 lead to α-helical content, which is comparable to experimental CD, and reproduce a theoretically expected β-sheet-turn-β-sheet conformational motif. Very recently, when we submitted this Article, Carballo-Pacheco et al. just reported MD simulations of five force fields (G54a7, OPLS, CHARMM22*, AMBER99SB*ILDN, and AMBER03WS) on hexamers of several Aβ_{16-22} peptides (wild-type and variants).[27] She suggested that G54a7 and OPLS are not ideal for studying Aβ_{16-22} oligomer formation and AMBER03WS is the only force field that works on aggregating and nonaggregating Aβ_{16-22} peptides. Their results suggest that the most suitable force field and water model for both folded and unfolded proteins remain to be identified.[15,23,83,84]

Taken together, the aforementioned force field benchmarks from us and others allow us to further narrow down our list of seven force fields to only five force fields. Those are A99SBi, A14SB, and the three CHARMM force fields (C22*, C36, C36m). These should be good candidates for the simulation of amyloid aggregation.

Convergence of conformational sampling is essential for any force field comparison studies; thus, most of the current studies employed the enhanced conformational sampling methods such as REMD, simulated tempering, and metadynamics. However, these techniques do not allow for obtaining the time scale of fibril formation, which is a very important parameter to the amyloid aggregation process and difficult to be obtained from experiments. In our case, we use multiple MD simulations starting from different structures and the small size of the dimer ensuring that the system reaches the equilibrium states within 200 ns. This allows us to calculate the fibril formation time directly from simulation trajectories. In general, the aggregation time not only depends on the total β-strand content but also the nucleation energy barrier that the system has to overcome for breaking any competing β-strand alignments and side-chain contacts.[85–87] As shown above, the fibril state of the Aβ_{16-22} dimer is determined by reaction coordinates q, which include the order parameter P_2, the β content of chains, and the interchain H-bonds. It is of interest to investigate which factors

control the fibril formation of the Aβ_{16-22} dimer. To this end, we plot the time evolution curves of P_2, the total number of the interchain H-bonds, and the β content of individual force fields (Figure S7). Then, we fit the data to a biexponential function taking the form of $q = a_0 + a_1 \exp\left(-\frac{t}{\tau_1}\right) + a_2 \exp\left(-\frac{t}{\tau_2}\right)$. The dominant value τ_i which corresponds to the largest weight a_i is related to the fibril formation time. We have found, and shown in Figure 3d, that the time scale associated with the time evolution of the β is not only close to the fibril formation time estimated directly from simulation trajectories for a given force field, but the trend is also similar between force fields. The fitted time scales of P_2 and interchain H-bonds behave differently and do not show any correlations with the fibril formation times. Taken together, our result suggests that the total β-strand content controls the fibril formation, at least for the Aβ_{16-22} dimer. This result, together with the fact that the A96, OPLS, and GROMOS family overestimate the β-content as shown above, suggests that the fibril formation and dissociation times shown in Figure 3d are probably overestimated. This is further supported by recent results of Strodel and colleagues showing that G54a7 and OPLS force fields overstabilize protein−protein interactions.[27]

CONCLUSION

In conclusion, our study provides for the first time ever the effects of 17 popular all-atom force fields of four families AMBER, CHARMM, OPLS, and GROMOS on the structure and kinetics of the model Aβ_{16-22} dimer. On the basis of this comparison and of the other published studies, we suggest that two AMBER force fields (A99SBi, A14SB) and the three CHARMM force fields (C22*, C36, C36m) are good candidates for the simulation of amyloid aggregation. We have also shown that the β-strand content is important for controlling the aggregation rates.

Supplementary Material

Refer to Web version on PubMed Central for supplementary material.

ACKNOWLEDGMENTS

Computational support from the Center for Research Computing of University of Pittsburgh, Pittsburgh Supercomputing Center (CHE180028P), the Extreme Science and Engineering Discovery Environment (CHE090098, MCB170099, and MCB180045P), and the supercomputer centers IDRIS, CINES (projects A0040710411 and A0030707721) are acknowledged.

Funding

This work was supported by grants R01-GM079383, R21-GM097617, and P30-DA035778 from the National Institutes of Health and CNRS. The content is solely the responsibility of the authors and does not necessarily represent the official views of the National Institutes of Health or other funding organizations. This work was supported by the Extreme Science and Engineering Discovery Environment (TGCHE090098) and the Center for Research Computing of University of Pittsburgh.

REFERENCES

(1). Sugita Y; Okamoto Y Replica-exchange molecular dynamics method for protein folding. Chem. Phys. Lett 1999, 314, 141.

(2). Zhang T; Nguyen PH; Nasica-Labouze J; Mu Y; Derreumaux P Folding atomistic proteins in explicit solvent using simulated tempering. J. Phys. Chem. B 2015, 119, 6941–6951. [PubMed: 25985144]

(3). Laio A; Parrinello M Escaping free-energy minima. Proc. Natl. Acad. Sci. U. S. A 2002, 99, 12562–12566. [PubMed: 12271136]

(4). Cornell WD; Cieplak P; Bayly CI; Gould IR; Merz KM; Ferguson DM; Spellmeyer DC; Fox T; Caldwell JW; Kollman PA A Second generation force field for the simulation of proteins, nucleic acids, and organic molecules. J. Am. Chem. Soc 1995, 117, 5179–5197.

(5). MacKerell ADM Jr; et al. All-atom empirical potential for molecular modeling and dynamics studies of proteins. J. Phys. Chem. B 1998, 102, 3586–3617. [PubMed: 24889800]

(6). van Gunsteren WF; Billeter SR; Eising AA; Hunenberger PH; Kruger P; Mark AE; Scott WRP; Tironi IG Biomolecular Simulation: The GROMOS96 Manual and User Guide, 1st ed.; Vdf Hochschulverlag AG an der ETH Zurich: Zurich, Switzerland, 1996.

(7). Kaminski GA; Friesner RA; Tirado-Rives J; Jorgensen WL Evaluation and reparameterization of the OPLS-AA force field for proteins via comparison with accurate quantum chemical calculations on peptides. J. Phys. Chem. B 2001, 105, 6474–6487.

(8). Ono S; Nakajima N; Higo J; Nakamura H Peptide free-energy profile is strongly dependent on the force field: Comparison of C96 and AMBER95. J. Comput. Chem 2000, 21, 748–762.

(9). Mu Y; Kosov DS; Stock G Conformational dynamics of trialanine in water. 2. Comparison of AMBER, CHARMM, GROMOS, and OPLS force fields to NMR and infrared experiments.J. Phys. Chem. B 2003, 107, 5064–5073.

(10). Yoda T; Sugita Y; Okamoto Y Comparisons of force fields for proteins by generalizedensemble simulations. Chem. Phys. Lett 2004, 386, 460–467.

(11). Gnanakaran S; García AE Helix-coil transition of alanine peptides in water: Force-field dependence on the folded and unfolded structures. Proteins: Struct., Funct., Genet 2005, 59, 773–782. [PubMed: 15815975]

(12). Matthes D; de Groot BL Secondary structure propensities in peptide folding simulations: A systematic comparison of molecular mechanics interaction schemes. Biophys. J 2009, 97, 599–608. [PubMed: 19619475]

(13). Sakae Y; Okamoto Y Folding simulations of three proteins having all α-helix, all β-strand and α/β-structures. Mol. Simul 2010, 36, 302–310.

(14). Robustelli P; Piana S; Shaw DE Developing a molecular dynamics force field for both folded and disordered protein states. Proc. Natl. Acad. Sci. U. S. A 2018, 115, E4758–E4766. [PubMed: 29735687]

(15). Cao Z; Liu L; Zhao L; Wang J Effects of different force fields and temperatures on the structural character of Abeta(12−28) peptide in aqueous solution. Int. J. Mol. Sci 2011, 12, 8259–8274. [PubMed: 22174662]

(16). Smith MD; Rao JS; Segelken E; Cruz L Force-field induced bias in the structure of Aβ21−30: A comparison of OPLS, AMBER, CHARMM, and GROMOS force fields. J. Chem. Inf. Model 2015, 55, 2587–2595. [PubMed: 26629886]

(17). Siwy CM; Lockhart C; Klimov DK Is the conformational ensemble of Alzheimer's Aβ10−40 peptide force field dependent? PLoS Comput. Biol 2017, 13, e1005314. [PubMed: 28085875]

(18). Gerben SR; Lemkul JA; Brown AM; Bevan DR Comparing atomistic molecular mechanics force fields for a difficult target: A case study on the Alzheimer's Amyloid β-peptide. J. Biomol. Struct. Dyn 2014, 32, 1817–1832. [PubMed: 24028075]

(19). Somavarapu AK; Kepp KP The dependence of Amyloid-β dynamics on protein force fields and water models. ChemPhysChem 2015, 16, 3278–3289. [PubMed: 26256268]

(20). Rosenman DJ; Wang C; García AE Characterization of Aβ monomers through the convergence of ensemble properties among simulations with multiple force fields. J. Phys. Chem. B 2016, 120, 259–277. [PubMed: 26562747]

(21). Carballo-Pacheco M; Strodel B Comparison of force fields for Alzheimer's Aβ_{42}: A case study for intrinsically disordered proteins. Protein Sci. 2017, 26, 174–185. [PubMed: 27727496]

(22). Weber OC; Uversky VN How accurate are your simulations? Effects of confined aqueous volume and AMBER FF99SB and CHARMM22/CMAP force field parameters on structural ensembles of intrinsically disordered proteins: Amyloid-β42 in water. Int. Dis. Pro 2017, 5, e1377813.

(23). Robustelli P; Piana S; Shaw DE Developing a molecular dynamics force field for both folded and disordered protein states. Proc. Natl. Acad. Sci. U. S. A 2018, 115, E4758–E4766. [PubMed: 29735687]

(24). Nguyen PH; Li MS; Derreumaux P Effects of all-atom force fields on Amyloid oligomerization: Replica Exchange Molecular Dynamics simulations of the Aβ_{16-22} Dimer and Trimer. Phys. Chem. Chem. Phys 2011, 13, 9778–788. [PubMed: 21487594]

(25). Watts CR; Gregory A; Frisbie C; Lovas S Effects of force fields on the conformational and dynamic properties of amyloid β(1−40) dimer explored by replica exchange molecular dynamics simulations. Proteins: Struct., Funct., Genet 2018, 86, 279–300. [PubMed: 29235155]

(26). Man VH; Nguyen PH; Derreumaux P High-resolution structures of the Amyloid-β_{1-42} dimers from the comparison of four atomistic force fields. J. Phys. Chem. B 2017, 121, 5977–5987. [PubMed: 28538095]

(27). Carballo-Pacheco M; Ahmed E; Ismail AE; Birgit Strodel B On the Applicability of Force Fields to Study the Aggregation of Amyloidogenic Peptides Using Molecular Dynamics Simulations. J. Chem. Theory Comput 2018, 14, 6063–6075. [PubMed: 30336669]

(28). Kollman PA Advances and continuing challenges in achieving realistic and predictive simulations of the properties of organic and biological molecules. Acc. Chem. Res 1996, 29, 461–469.

(29). Wang J; Cieplak P; Kollman PA How well does a restrained electrostatic potential (RESP) model perform in calculating conformational energies of organic and biological molecules? J. Comput. Chem 2000, 21, 1049–1074.

(30). Lindorff-Larsen K; Piana S; Palmo K; Maragakis P; Klepeis JL; Dror RO; Shaw DE Improved side-chain torsion potentials for the AMBER99SB protein force field. Proteins: Struct., Funct., Genet 2010, 78, 1950. [PubMed: 20408171]

(31). Duan Y; Wu C; Chowdhury S; Lee MC; Xiong G; Zhang W; Yang R; Cieplak P; Luo R; Lee T; Caldwell J; Wang J; Kollman P A point-charge force field for molecular mechanics simulations of proteins based on condensed-phase quantum mechanical calculations. J. Comput. Chem 2003, 24, 1999–2012. [PubMed: 14531054]

(32). Maier JA; Martinez C; Kasavajhala K; Wickstrom L; Hauser KE; Simmerling C ff14SB: Improving the accuracy of protein side chain and backbone parameters from ff99SB. J. Chem. Theory Comput 2015, 11, 3696–3713. [PubMed: 26574453]

(33). Piana S; Lindorff-Larsen K; Shaw DE How robust are protein folding simulations with respect to force field parameterization? Biophys. J 2011, 100, L47–L49. [PubMed: 21539772]

(34). Best RB; Zhu X; Shim J; Lopes PEM; Mittal J; Feig M; MacKerell AD Jr. Optimization of the additive CHARMM all-atom protein force field targeting improved sampling of the backbone φ, ψ and side-chain χ1 and χ2 dihedral angles. J. Chem. Theory Comput 2012, 8, 3257–3273. [PubMed: 23341755]

(35). Huang J; Rauscher S; Nawrocki G; Ran T; Feig M; de Groot BL; Grubmüller H; MacKerell AD CHARMM36m: An improved force field for folded and intrinsically disordered proteins. Nat. Methods 2017, 14, 71–73. [PubMed: 27819658]

(36). Daura X; Mark AE; Gunsteren WFV Parametrization of aliphatic CH_n united atoms of GROMOS96 force field. J. Comput. Chem 1998, 19, 535–547.

(37). Schuler LD; van Gunsteren WF On the choice of dihedral angle potential energy functions for n-Alkanes. Mol. Simul 2000, 25, 301–319.

(38). Schuler LD; Daura X; van Gunsteren WF An improved GROMOS96 force field for aliphatic hydrocarbons in the condensed phase. J. Comput. Chem 2001, 22, 1205–1218.

(39). Oostenbrink C; Villa A; Mark AE; Gunsteren WFV A biomolecular force field based on the free enthalpy of hydration and solvation: the GROMOS force-field parameter sets 53A5 and 53A6. J. Comput. Chem 2004, 25, 1656–1676. [PubMed: 15264259]

(40). Schmid N; Eichenberger AP; Choutko A; Winger SR; Mark AE; van Gunsteren WF Definition and testing of the GROMOS force-field versions 54A7 and 54B7. Eur. Biophys. J 2011, 40, 843–856. [PubMed: 21533652]

(41). Kirschner DA; Inouye H; Duffy LK; Sinclair A; Lind M; Selkoe DJ Synthetic peptide homologous to beta protein from Alzheimer disease forms amyloid-like fibrils in vitro. Proc. Natl. Acad. Sci. U. S. A 1987, 84, 6953–7. [PubMed: 3477820]

(42). Wood SJ; Wetzel R; Martin JD; Hurle MR Prolines and amyloidogenicity in fragments of the Alzheimer's peptide beta/A4. Biochemistry 1995, 34, 724–30. [PubMed: 7827029]

(43). Fay DS; Fluet A; Johnson CJ; Link CD In vivo aggregation of beta-amyloid peptide variants. J. Neurochem 1998, 71, 1616–25. [PubMed: 9751195]

(44). Tjernberg LO; Näslund J; Lindqvist F; Johansson J; Karlström AR; Thyberg J; Terenius L; Nordstedt C Arrest of beta-amyloid fibril formation by a pentapeptide ligand. J. Biol. Chem 1996, 271, 8545–8. [PubMed: 8621479]

(45). Ma B; Nussinov R Simulations as analytical tools to understand protein aggregation and predict amyloid conformation. Curr. Opin. Chem. Biol 2006, 10, 445–452. [PubMed: 16935548]

(46). Chebaro Y; Mousseau N; Derreumaux P Structures and thermodynamics of Alzheimer's Amyloid-β Aβ_{16-35} monomer and dimer by Replica Exchange Molecular Dynamics simulations: Implication for full-length Abeta fibrillation. J. Phys. Chem. B 2009, 113, 7668–7675. [PubMed: 19415895]

(47). Balbach JJ; Ishii Y; Antzutkin ON; Leapman RD; Rizzo NW; Dyda F; Reed J; Tycko R Amyloid fibril formation by Aβ_{16-22}, a seven-residue fragment of the Alzheimer's β-Amyloid peptide, and structural characterization by solid state NMR. Biochemistry 2000, 39, 13748–13759. [PubMed: 11076514]

(48). Klimov DK; Thirumalai D Dissecting the assembly of Abeta(16−22) amyloid peptides into antiparallel beta sheets. Structure 2003, 11, 295–307. [PubMed: 12623017]

(49). Gnanakaran S; Nussinov R; Garcia AE Atomic-level description of Amyloid β-dimer formation. J. Am. Chem. Soc 2006, 128, 2158–2159. [PubMed: 16478138]

(50). Nguyen PH; Li MS; Stock G; Straub JE; Thirumalai D Monomer adds to preformed structured oligomers of Aβ-peptides by a two-stage dock-lock mechanism. Proc. Natl. Acad. Sci. U. S. A 2007, 104, 111–116. [PubMed: 17190811]

(51). Barz B; Wales DJ; Strodel B A Kinetic Approach to the Sequence−Aggregation Relationship in Disease-Related Protein Assembly. J. Phys. Chem. B 2014, 118, 1003–1011. [PubMed: 24401100]

(52). Favrin G; Irbäck A; Mohanty S Oligomerization of amyloid Aβ_{16-22} peptides using hydrogen bonds and hydrophobicity forces. Biophys. J 2004, 87, 3657–3664. [PubMed: 15377534]

(53). Santini S; Mousseau N; Derreumaux P In Silico assembly of Alzheimer's Aβ_{16-22} Peptide into β-Sheets. J. Am. Chem. Soc 2004, 126, 11509–11516. [PubMed: 15366896]

(54). Santini S; Wei G; Mousseau N; Derreumaux P Pathway complexity of Alzheimer's β-Amyloid Aβ_{16-22} peptide assembly. Structure 2004, 12, 1245–1255. [PubMed: 15242601]

(55). Derreumaux P; Mousseau N Coarse-grained protein molecular dynamics simulations. J. Chem. Phys 2007, 126, 025101–025106. [PubMed: 17228975]

(56). Lu Y; Derreumaux P; Guo Z; Mousseau N; Wei G Thermodynamics and dynamics of amyloid peptide oligomerization are sequence dependent. Proteins: Struct., Funct., Genet 2009, 75, 954–963. [PubMed: 19089954]

(57). Tran TT; Nguyen PH; Derreumaux P Lattice model for amyloid peptides: OPEP force field parametrization and applications to the nucleus size of Alzheimer's peptides. J. Chem. Phys 2016, 144, 205103. [PubMed: 27250331]

(58). van Gunsteren W; Billeter SR; Eising AA; Hünenberger PH; Krüger P; Mark AE; Scott W; Tironi I Biomolecular Simulation: The GROMOS96 Manual and User Guide; Vdf Hochschulverlag AG an der ETH: Zurich, Switzerland, 1996.

(59). Zhang S; Iwata K; Lachenmann MJ; Peng JW; Li S; Stimson ER; Lu Y; Felix AM; Maggio JE; Lee JP The Alzheimer's peptide Aβ adopts a collapsed coil structure in water. J. Struct. Biol 2000, 130, 130–141. [PubMed: 10940221]

(60). Jorgensen WL; Chandrasekhar J; Madura JD; Impey RW; Klein ML Comparison of simple potential functions for simulating liquid water. J. Chem. Phys 1983, 79, 926–935.

(61). Berendsen HJC; Postma JPM; van Gunsteren WF; Dinola A; Haak JR Molecular dynamics with coupling to an external bath. J. Chem. Phys 1984, 81, 3684–3690.

(62). Bussi G; Donadio D; Parrinello M Canonical sampling through velocity rescaling. J. Chem. Phys 2007, 126, 014101. [PubMed: 17212484]

(63). Hess B; Kutzner C; van der Spoel D; Lindahl E Gromacs 4: Algorithms for highly efficient, load-balanced, and scalable molecular simulation. J. Chem. Theory Comput 2008, 4, 435–447. [PubMed: 26620784]

(64). Hockney RW; Goel SP; Eastwood J Quit high resolution computer models of plasma. J. Comput. Phys 1974, 14, 148–158.

(65). Hess B; Bekker H; Berendsen HJC; Fraaije JGEM LINCS: A linear constraint solver for molecular simulations. J. Comput. Chem 1997, 18, 1463–1472.

(66). Darden T; York D; Pedersen L Particle mesh Ewald: An Nlog(N) method for Ewald sums in large systems. J. Chem. Phys 1993, 98, 10089–10092.

(67). Frishman D; Argos P Knowledge-based secondary structure assignment. Proteins: Struct., Funct., Genet 1995, 23, 566–579. [PubMed: 8749853]

(68). Heinig M; Frishman D STRIDE: a Web server for secondary structure assignment from known atomic coordinates of proteins. Nucleic Acids Res. 2004, 32, W500–2. [PubMed: 15215436]

(69). Cecchini M; Rao F; Seeber M; Caflisch A Replica exchange molecular dynamics simulations of amyloid peptide aggregation. J. Chem. Phys 2004, 121, 10748–10756. [PubMed: 15549960]

(70). Petkova AT; Buntkowsky G; Dyda F; Leapman RD; Yau WM; Tycko R Solid state NMR reveals a pH-dependent antiparallel beta-sheet registry in fibrils formed by a beta-amyloid peptide. J. Mol. Biol 2004, 335, 247–260. [PubMed: 14659754]

(71). Rohrig UF; Laio A; Tantalo N; Parrinello M; Petronzio R Stability and structure of oligomers of the Alzheimer peptide Aβ_{16}−22: From the dimer to the 32-Mer. Biophys. J 2006, 91, 3217–3222. [PubMed: 16920832]

(72). Wei G; Mousseau N; Derreumaux P Computational simulations of the early steps of protein aggregation. Prion 2007, 1, 3–8. [PubMed: 19164927]

(73). MacKerell AD; et al. All-atom empirical potential for molecular modeling and dynamics studies of proteins. J. Phys. Chem. B 1998, 102, 3586–3616. [PubMed: 24889800]

(74). MacKerell AD; Feig M; Brooks CL Extending the treatment of backbone energetics in protein force fields: Limitations of Gas-Phase quantum mechanics in reproducing protein conformational distributions in molecular dynamics simulations. J. Comput. Chem 2004, 25, 1400–1415. [PubMed: 15185334]

(75). Brooks BR; et al. CHARMM: The biomolecular simulation program. J. Comput. Chem 2009, 30, 1545–1614. [PubMed: 19444816]

(76). Jensen KP; Jorgensen WL Halide, Ammonium, and Alkali Metal Ion parameters for modeling aqueous solutions. J. Chem. Theory Comput 2006, 2, 1499–1509. [PubMed: 26627020]

(77). Jensen KP Improved Interaction Potentials for Charged Residues in Proteins. J. Phys. Chem. B 2008, 112, 1820–1827. [PubMed: 18205348]

(78). Berendsen H; Postma J; van Gunsteren W; Hermans J In Intermolecular Forces; Reidel: 1981.

(79). Hornak V; Abel R; Okur A; Strockbine B; Roitberg A; Simmerling C Comparison of multiple Amber force fields and development of improved protein backbone parameters. Proteins: Struct., Funct., Genet 2006, 65, 712–725. [PubMed: 16981200]

(80). Best RB; Hummer G Optimized molecular dynamics force fields applied to the helix-coil transition of polypeptides. J. Phys. Chem. B 2009, 113, 9004–9015. [PubMed: 19514729]

(81). Li D; Brüschweiler R NMR-based protein potentials. Angew. Chem., Int. Ed 2010, 49, 6778–80.

(82). Best RB; Zheng W; Mittal J Balanced Protein-Water Interactions Improve Properties of Disordered Proteins and Non-Specific Protein Association. J. Chem. Theory Comput 2014, 10, 5113–5124. [PubMed: 25400522]

(83). Nasica-Labouze J; et al. Amyloid β Protein and Alzheimer's Disease: When Computer Simulations Complement Experimental Studies. Chem. Rev 2015, 115, 3518–3563. [PubMed: 25789869]

(84). Doig AJ; Del Castillo-Frias MP; Berthoumieu O; Tarus B; Nasica-Labouze J; Sterpone F; Nguyen PH; Hooper NM; Faller P; Derreumaux P Why Is Research on Amyloid-β Failing to

Give New Drugs for Alzheimer's Disease? ACS Chem. Neurosci 2017, 8, 1435–1437. [PubMed: 28586203]

(85). Co NT; Li MS New method for determining size of critical nucleus of fibril formation of polypeptide chains. J. Chem. Phys 2012, 137, 095101. [PubMed: 22957596]

(86). Reddy G; Straub JE; Thirumalai D Influence of preformed Asp23-Lys28 salt bridge on the conformational fluctuations of monomers and dimers of Aβ peptides with implications for rates of fibril formation. J. Phys. Chem. B 2009, 113, 1162–1172. [PubMed: 19125574]

(87). Ball KA; Phillips AH; Wemmer DE; Head-Gordon T Differences in β-strand populations of monomeric Aβ40 and Aβ42. Biophys. J 2013, 104, 2714–2724. [PubMed: 23790380]

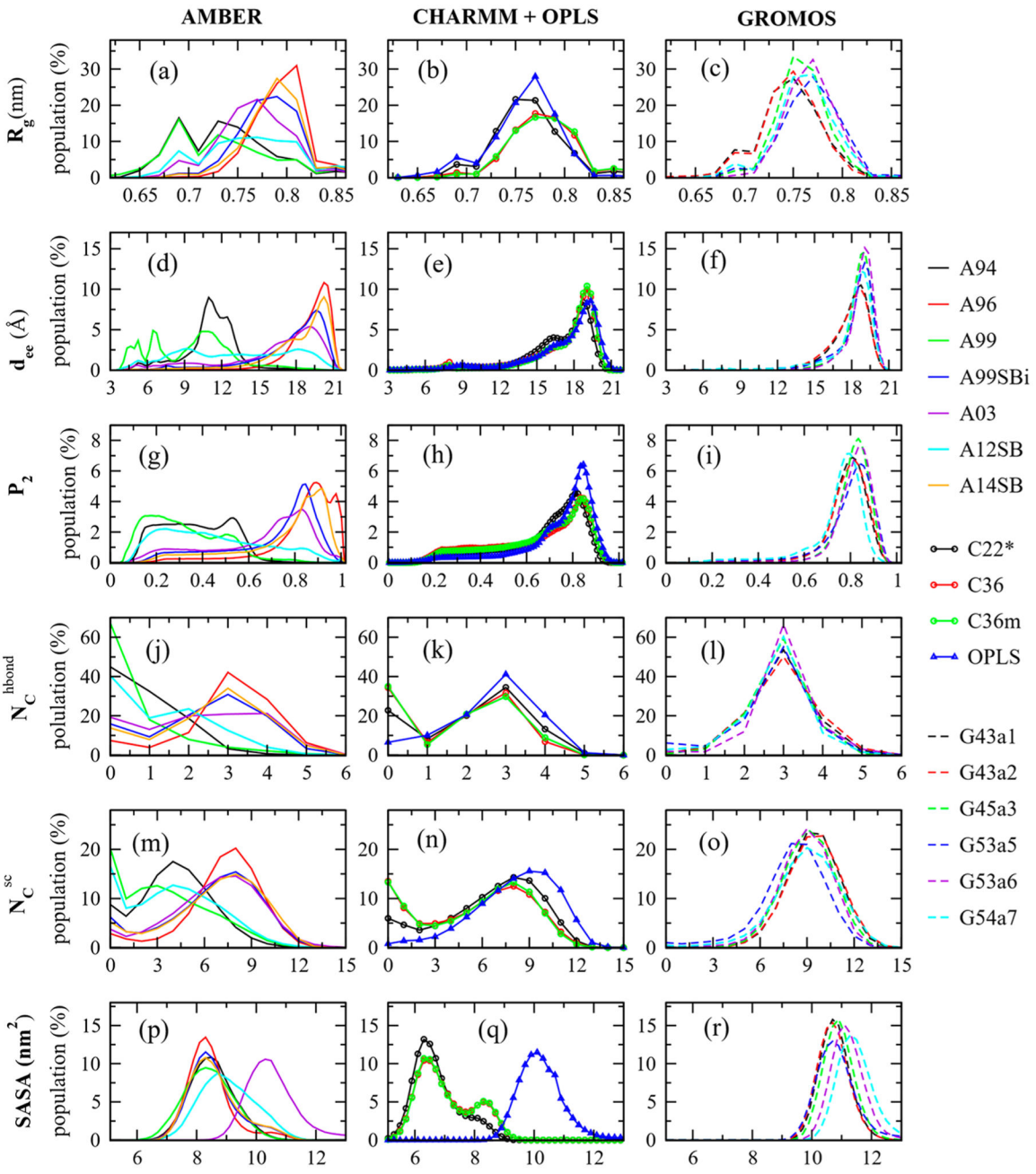

Figure 1.

Normalized distributions of the radius of gyration (R_g), the end-to-end distance (d_{ee}), the order parameter (P_2), the intermolecular backbone H-bonds (N^{hbond}_C), the intermolecular side chain−side chain contacts (N^{sc}_C), and the solvent accessible surface area (SASA). Shown are results obtained by AMBER, CHARMM, OPLS, and GROMOS force field families and averaged over all conformations.

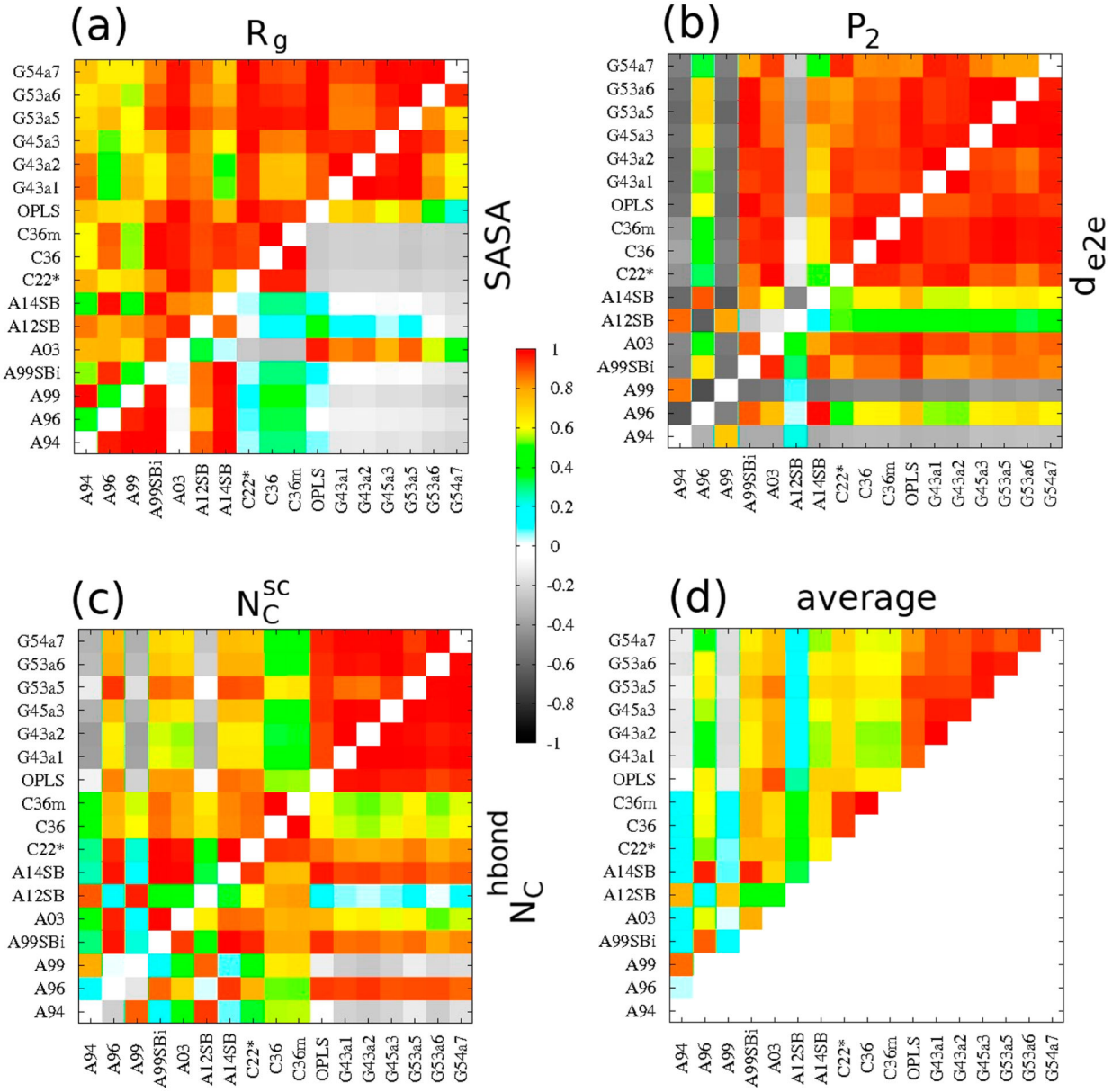

Figure 2.

Map of the Pearson correlation coefficient between the force fields, which are calculated from the distributions of the R_g (upper-left triangle) and SASA (lower-right triangle) shown in part a, the P_2 (upper-left triangle) and d_{ee} (lower-right triangle) shown in part b, and the $N^{sc}{}_C$ (upper-left triangle) and $N^{hbond}{}_C$ (lower-right triangle) shown in part c. The map of the Pearson correlation coefficient averaged over the six above reaction coordinates is shown in part d.

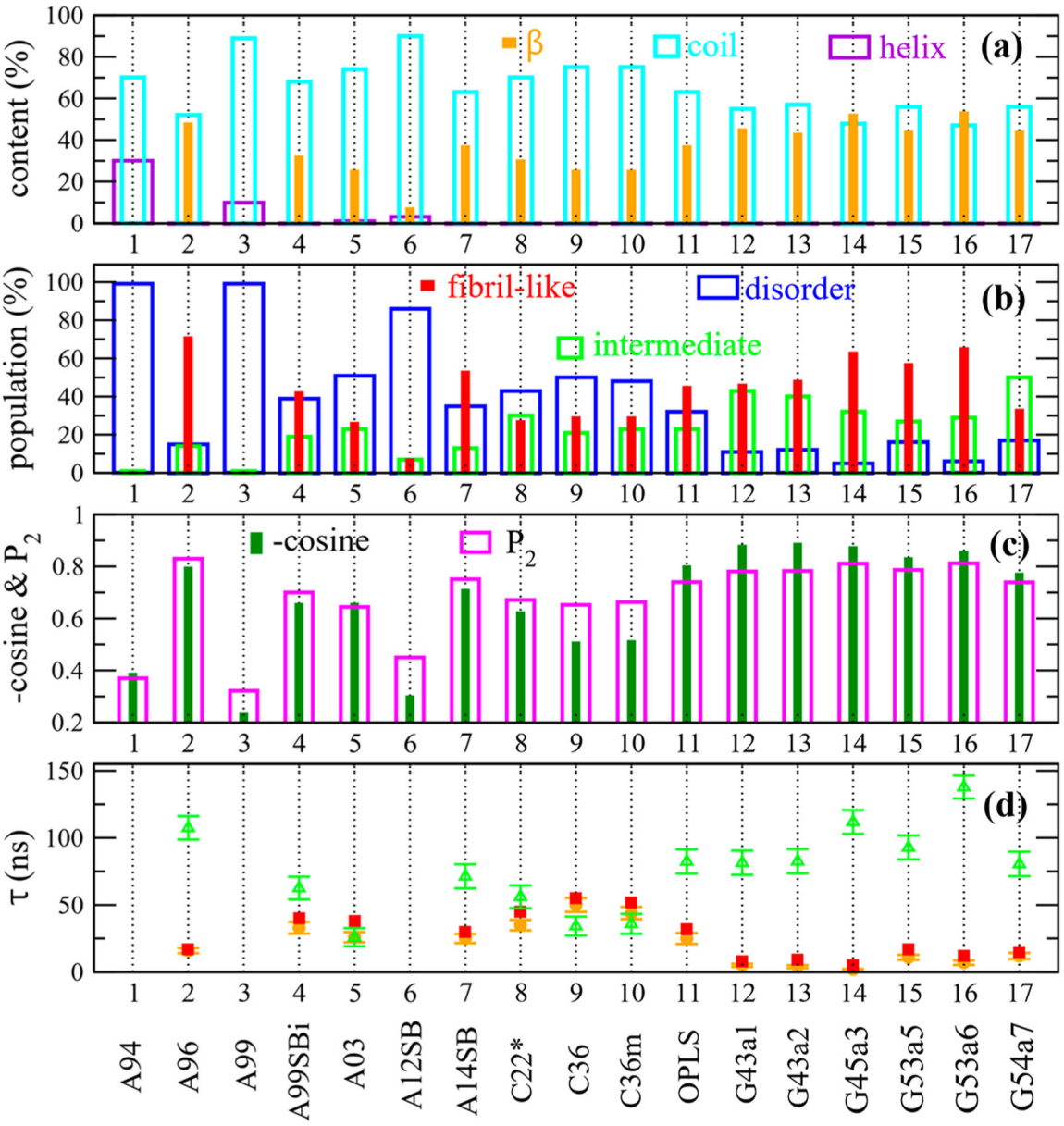

Figure 3.

Mean values of various quantities as a function of force fields, including the population of the β, helix, and coil structures (a), the population of the disordered, intermediate, and fibril states (b), the −cosine and P_2 between two chains (c), and the fibril formation time (orange) and fibril dissociation time (green) (d). In part d, the red square dots represent the time obtained from biexponential fits of the time evolution of the β content. Shown are results averaged over 200 ns and 100 trajectories.

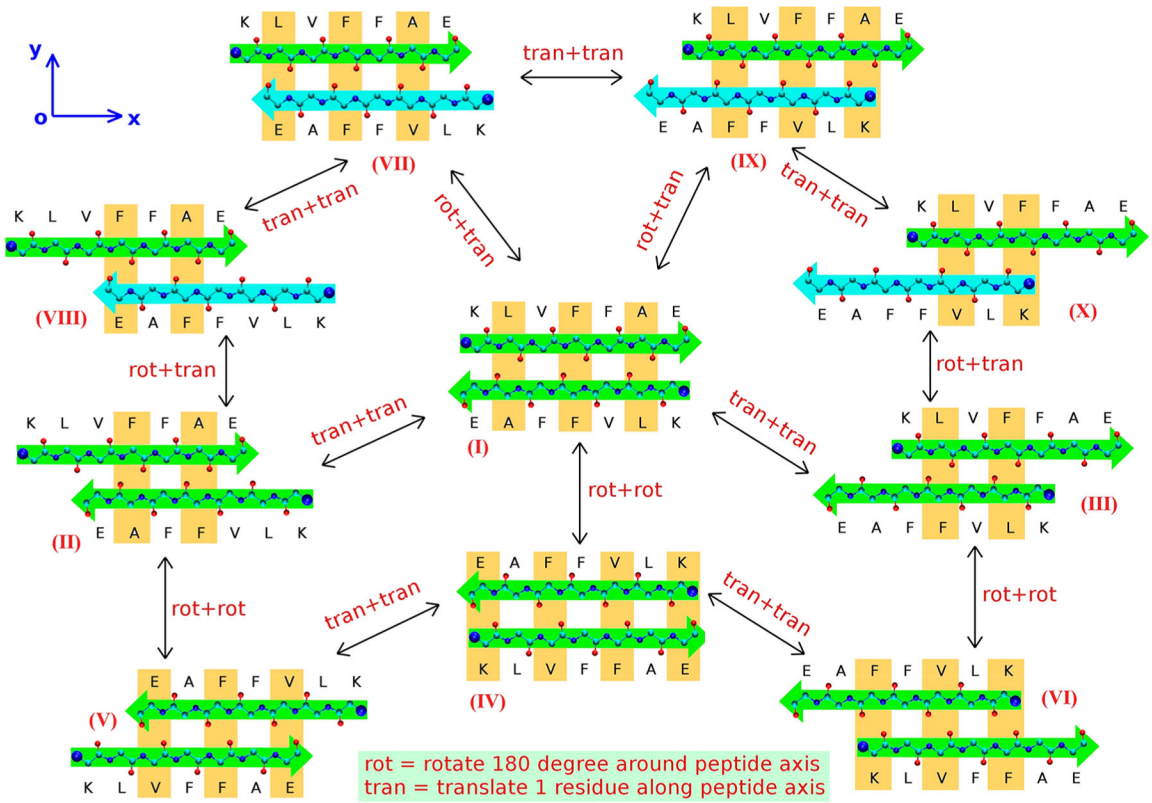

Figure 4.

Ten possible antiparallel β-sheet registries of Aβ_{16-22} dimer. The green and cyan arrows indicate the face-in and face-out of the peptide with respect to the plotted plane, respectively. The peptide backbone is shown in VMD CPK representation with the blue, red, and cyan balls representing the N, O, and C atoms, respectively. The interpeptide H-bond pattern is marked by an orange rectangle. See the text for a detailed explanation of different registries.

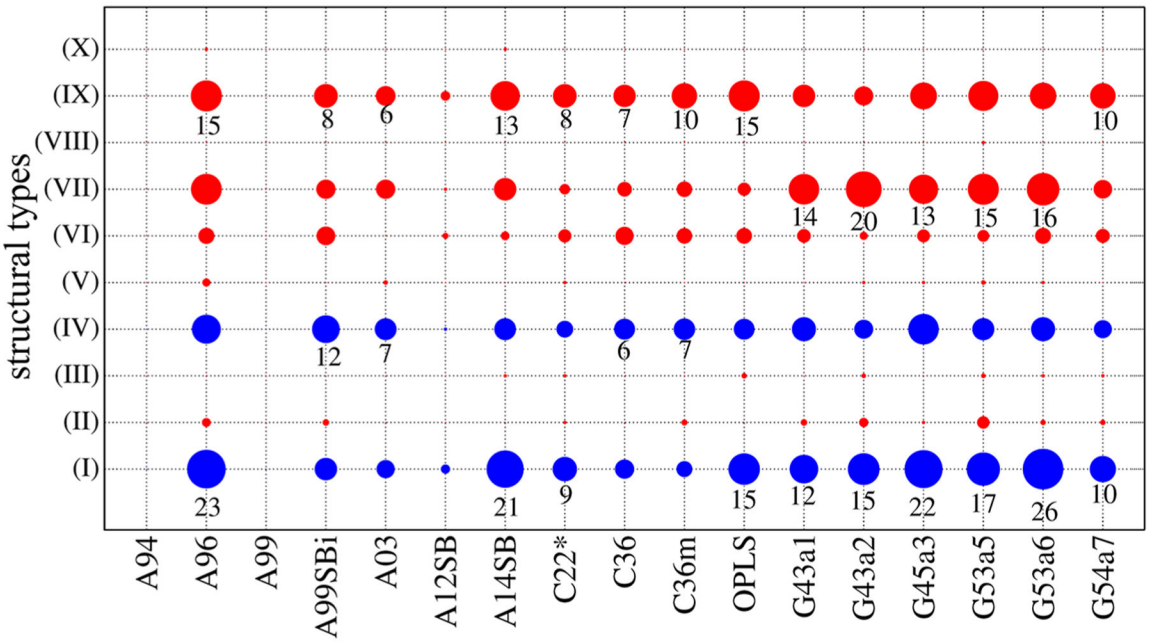

Figure 5.

Population, represented by circles, of the antiparallel β-sheets having different H-bond patterns. The blue and red circles indicate the in-register and out-of-register patterns, respectively. The circle size is proportional to the population. Shown are results obtained from all conformations in 100 trajectories and 200 ns for each force field.

Table 1.

Summary of the Explicit-Solvent All-Atoms Force Field Comparison Studies on Aβ[a]

Refs	system	Method	Compared force fields	Exp. data
15	$A\beta_{12-28}$	0.03μs × 36 rep	GROMOS-43A1 and OPLS-AA	
16	$A\beta_{21-30}$	0.5 μs × 15 sim	AMBER99, AMBER99SB, AMBER99SB-ILDN and AMBERO, CHARMM22*, GROMOS-53A6 and OPLS-AA	
17	$A\beta_{10-40}$	0.08 μs × 40 rep	CHARMM22*, CHARMM22+CMAP, CHARMM36 and OPLS-AA	J-couplingand RDC
18	$A\beta_{1-40}$	0.44 μs × 3 sim	AMBER03, GROMOS-54A7, GROMOS-53A6, CHARM22+CMAP and OPLS-AA	SS and CS
19	$A\beta_{1-40}$	0.8 μs × 4 sim	AMBER03, AMBER99SB-ILDN, CHARMM27, CHARMM22*, GROMOS-43A1, GROMOS-53A6, GROMOS-54A7, OPLS-AA, OPLS-2006 and OPLS-2008	NMR and CD
23	$A\beta_{1-40}$	30 μs	AMBER99SB-ILDN, AMBER99SB* ILDN, AMBER99SB-UCB, AMBER99SB-disp, AMBER03WS, CHARMM22*, CHARMM36m	CS, RDC, J-coupling and R_g
20	$A\beta_{1-40}$ $A\beta_{1-42}$	1 μs × 52 rep	AMBER99SB-ILDN, CHARMM22* and OPLS-AA	SS, CS and J-coupling
21	$A\beta_{1-42}$	0.2 μs × 32 rep	AMBER99SB, AMBER99SB*ILDN, AMBER99SB-ILDN-NMR, CHARMM22* and OPLS-AA	CS
22	$A\beta_{1-42}$	0.225 μs × 32 rep	CHARMM22+CMAP and AMBER99SB	SS and CS
24	$A\beta_{16-22}$ $\{A\beta_{16-22}\}_2$ $\{A\beta_{16-22}\}_3$	0.5 μs × 1 sim 0.055 μs × 32 rep 0.055 μs × 40 rep	AMBER99, GROMOS-43A1 and OPLS-AA	
26	$\{A\beta_{1-42}\}_2$	0.75 μs × 48 rep	AMBER99SB-ILDN, AMBER14SB, CHARMM22* and OPLS-AA	SS, CD and CCS
25	$\{A\beta_{1-40}\}_2$	0.3 μs × 70 rep	AMBER99SB-ILDN, AMBER99SB-ILDN*, AMBER99SB-ILDN-NMR, CHARMM22* and CHARMM36	
27	$\{A\beta_{16-22}\}_6$	0.3÷1 μs × 5 sim	GROMOS54a7, OPLS, AMBER03WS, AMBER99SB*ILDN, CHARMM22*	K_D

[a]Here, “rep” and “sim” indicate the number of replicas (in REMD) and number of MD simulations (or run), respectively. “SS”, “CS”, “CD”, “RDC”, “NMR”, “CCS”, and K_D are abbreviations for secondary structure, chemical shifts, circular dichroism spectrum, residual dipolar coupling, nuclear magnetic resonance spectrum, collision cross section, and the dissociation constant, respectively. The force fields are colored in blue if the authors concluded that their findings are consistent with experimental data.

J Chem Theory Comput. Author manuscript; available in PMC 2019 September 16.